PHYSICAL REVIEW C VOLUME 25, NUMBER 5 MAY 1982

Large angle elastic and inelastic scattering of protons from ^{40}Ca at 800 MeV

E. Bleszynski, M. Bleszynski, S. Hajisaeid, G. J. Igo, F. Irom, J. B. McClelland,[*]
G. Pauletta, A. Rahbar, A. T. M. Wang, C. A. Whitten, Jr., and G. Adams[†]
University of California, Los Angeles, California 90024

M. Barlett, G. W. Hoffmann, and J. A. McGill
University of Texas, Austin, Texas 78712

R. Boudrie
University of California, Los Alamos National Laboratory, Los Alamos, New Mexico 87545

G. Kyle[‡]
University of Minnesota, Minneapolis, Minnesota 55455
(Received 22 September 1981)

Measurements are reported for the elastic and inelastic scattering of 800 MeV protons from ^{40}Ca. Differential cross sections were measured out to 42° while analyzing powers were obtained out to 30°. The angular distributions are diffractive in character at all angles. Theoretical analysis of the data was carried out in the framework of the diffraction multiple scattering theory. The following results were obtained: (i) Diffraction multiple scattering theory reproduces the data qualitatively out to the large momentum transfers. (ii) For the ground state density distribution $\langle r_p{}^2\rangle^{1/2}-\langle r_n{}^2\rangle^{1/2}=0.142\pm0.075$ fm is obtained and the analysis favors the value of the correlation length $\xi_c=-0.5$ fm. (iii) The excitation of the lowest-lying collective states (3^-, 5^-, 2^+) was analyzed using one-phonon excitation macroscopic parameters. The values of the β_2, β_3, β_5 parameters obtained agree quantitatively with lower energy (p,p') scattering results.

NUCLEAR REACTIONS ^{40}Ca(p,p), ^{40}Ca(p,p'), $E=0.8$ GeV, proton elastic and inelastic scattering cross sections and analyzing powers, target ^{40}Ca, $E_{\text{lab}}=0.8$ GeV, $\theta_{\text{c.m.}}=2.5°-42°$, Glauber diffraction scattering theory, deduced Δr_{np}, transition strengths.

I. INTRODUCTION

In this paper we present the results of new experimental and theoretical work on the large angle elastic and inelastic scattering of 800 MeV protons from ^{40}Ca. The high resolution spectrometer (HRS) at the Clinton P. Anderson Meson Physics Facility (LAMPF) was used to obtain the data. The elastic differential cross section was measured from 2° out to 42° in the center of mass frame (c.m.f.), which considerably exceeds the angular range covered by the previous experiments[1,2] which extended only to 24° in the c.m.f. The differential cross sections for the inelastic transitions to the 3.74 MeV (3^-) and 4.49 MeV (5^-) states of ^{40}Ca were measured out to 42°. The transition to the 3.9 MeV (2^+) state was measured out to 30°. We also report the proton analyzing powers for these elastic and inelastic transitions for the 2°−30° angular range. The statistical errors in the angular distribution of the elastic cross section are typically $\pm1\%$, except at the largest angles, whereas those of the analyzing powers vary between ±0.01 and ±0.05. The absolute scattering angle was determined to $\pm0.03°$. The normalization uncertainty of the cross section is $\pm10\%$.

The data are compared with the predictions of the Glauber diffraction multiple scattering theory.[3] The finite energy noneikonal corrections were calculated using the approach of Bleszynski and Osland.[4]

Very good agreement at large momentum transfers, between the data and the present calculation, can be qualitatively understood by recognizing that although the total momentum transfer is rather large, the multiple scattering proceeds through a series of small momentum transfer collisions.

In Sec. II details of the experiment are discussed. Section III is devoted to the theoretical analysis and comparison of the theoretical results with the experimental data. Finally, a summary and conclusions are given in Sec. IV.

II. EXPERIMENTAL METHOD AND DISCUSSION OF EXPERIMENTAL RESULTS

The elastic and inelastic scattering of 800 MeV protons from ^{40}Ca has been studied over a relatively broad range of scattering angles (out to 42° c.m.). At 42° in the center of mass the elastic scattering cross section is ~ 1 nb/sr which, at the present time, is the limiting measurable value (due to background) at the HRS facility at LAMPF.

The unpolarized differential cross section data were taken in conjunction with similar measurements on ^{208}Pb, and the experimental details for this part of the work are exhaustively described in a paper[5] reporting the ^{208}Pb elastic scattering results and will not be discussed here except as they pertain specifically to the ^{40}Ca measurement. The large angle $\vec{p}+{}^{208}$Pb analyzing power data are reported in Ref. 6.

Since our object was to investigate large momentum transfers (large scattering angles) for elastic scattering and inelastic excitations, we maintained good energy resolution in order to pick out small yield peaks on a substantial background. The energy resolution was ≤ 150 keV at most angles. Running periods with unpolarized beam at the larger angles were extended up to 8 h, utilizing a 50 nA beam and a target of several hundred mg/cm^2. The measurements were discontinued when it was no longer possible to discern a significant yield above the background in reasonable running periods. In the case of the measurements with polarized beams, data were obtained out to 30 deg. The method of data analysis in both measurements also did not differ substantially from the method described earlier.[1,2,5,6]

Figures 1—3 show spectra obtained at different angles. At small angles (Fig. 1), the spectra contain many known states and, in addition, some rather strongly excited states or groups of states at large excitations which cannot be identified uniquely. The elastic peak generally dominates the spectrum in this region. Among the inelastic excitations, the lowest 3^- (3.74 MeV) and 5^- (4.49 MeV) collective states are the strongest excited.

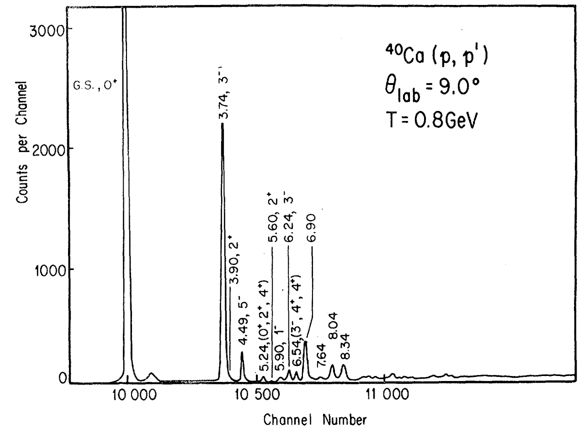

FIG. 1. The spectrum of 800 MeV protons scattered from ^{40}Ca at 9° (identified by their energies in MeV). The energy scale is 10 keV per channel.

At intermediate angles (Fig. 2), most of the states seen in Fig. 1 are no longer discernible. The spectrum is now clearly dominated by the low lying collective 3^- state. The lowest lying 5^- state is also excited, and a state or group of states near 6.9 MeV excitation is the other clear feature. The angular distribution of the latter is consistent with a combination of two or more states being populated, including a 2^+ and a higher spin state. The former has been previously identified at this excitation.[7] Finally, in Fig. 3, taken at nearly the largest angle

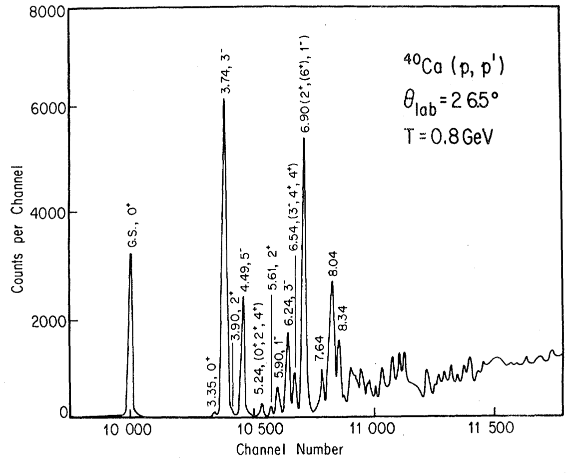

FIG. 2. The spectrum of 800 MeV protons scattered from ^{40}Ca at 26.5° (identified by their energies in MeV). The energy scale is 10 keV per channel.

investigated, the elastic and 5^- excitations have become relatively small. The 3^- and the 6.9 MeV cluster continue to dominate the spectrum.

The multiple scattering calculations presented in this paper readily predict the right order of magnitude for the cross section and polarization of the 2^+, 3^-, and 5^- states. The elastic differential cross section $(d\sigma/d\Omega)$ and analyzing power $A(\theta)$ are displayed in Figs. 4 and 5. The inelastic excitation of the 2^+ state (3.90 MeV) is shown in Figs. 6 and 7; the 3^- state (3.74 MeV), in Figs. 8 and 9; and the 5^- state (4.49 MeV), in Figs. 10 and 11. A complete tabulation of the elastic and inelastic data is on deposit in PAPS.[37]

III. THEORETICAL ANALYSIS

A. Elastic scattering

1. *Formalism*

We have carried out the theoretical analysis of the elastic scattering differential cross section using the high energy Glauber diffraction theory[3] with finite energy noneikonal corrections calculated according to Ref. 4.

In this approach the amplitude of the elastic scattering of a projectile (proton) from the nucleus can be expressed in terms of the on-shell projectile-target elementary amplitudes and the target ground state density:

$$F_{00}(\vec{\Delta})=\frac{ik}{2\pi}\int d^2b\, e^{i\vec{\Delta}\cdot\vec{b}}\int d^3r_1\ldots d^3r_A\,\rho(\vec{r}_1\ldots\vec{r}_A)\tilde{\Gamma}(\vec{b},\vec{r}_1\ldots\vec{r}_A)\,, \tag{1}$$

where k is the projectile laboratory momentum, $\vec{\Delta}$ is the momentum transfer, and $\tilde{\Gamma}$ is the nucleus profile function. The Glauber approach itself is essentially a high energy and small scattering angle approximation, based on the assumption of straight line propagation of the incident projectile. The data reported here were taken at intermediate energy, where deviations from the straight line projectile propagation (i.e., noneikonal effects) become important. Hence inclusion of these effects in our calculation should provide us with a more accurate description of the data.

Inclusion of the noneikonal effects, according to Ref. 4, leads us to the following expression for the nucleus profile function $\tilde{\Gamma}$:

$$\tilde{\Gamma}(\vec{b},\vec{s}_1,\ldots\vec{s}_A)=\Gamma(\vec{b},\vec{s}_1,\ldots\vec{s}_A)+\delta\Gamma_{\rm noneik}(\vec{b},\vec{s}_1,\ldots\vec{s}_A) \tag{2}$$

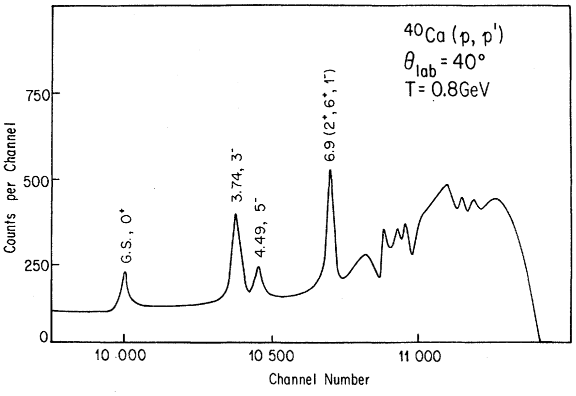

FIG. 3. The spectrum of 800 MeV protons scattered from ^{40}Ca at 40° (identified by their energies in MeV). The energy scale is 10 keV per channel.

with

$$\Gamma(b,\vec{s}_1,\ldots\vec{s}_A)=1-\prod_{i/1}^{A}[1-\gamma(\vec{b}-\vec{s}_i)]\,, \tag{3}$$

where γ is the two-dimensional Fourier transform of the elementary projectile (proton)-target nucleon amplitudes, and $\delta\Gamma_{\rm noneik}$ is the noneikonal correction to the Glauber model profile function [see Eq.

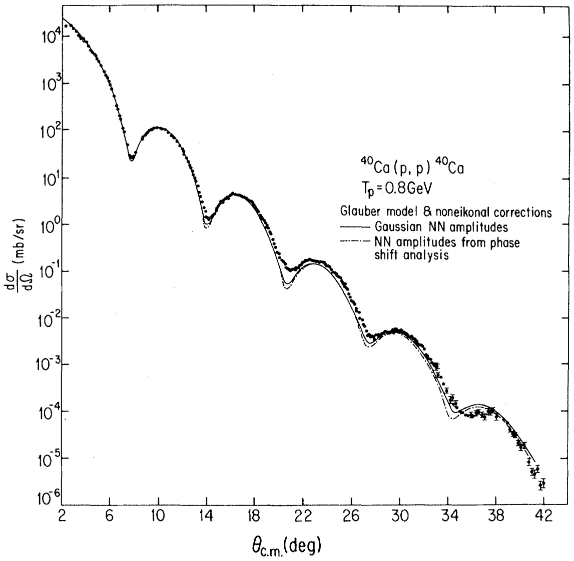

FIG. 4. Differential cross section for the elastic p-^{40}Ca scattering at 800 MeV. Both curves represent the results of the full calculation described in the text. The solid curve corresponds to the Gaussian parametrization of the pp and pn amplitudes, the dashed-dotted curve was obtained with the pp and pn amplitudes taken from phase shift analysis (Ref. 26).

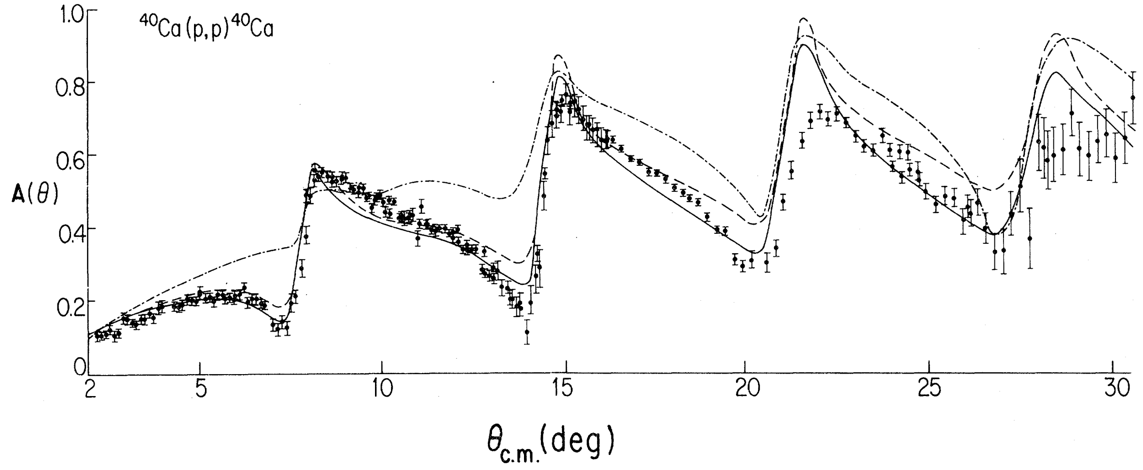

FIG. 5. Analyzing power in the elastic p-^{40}Ca scattering at 800 MeV. The dashed and solid curves illustrate the effect of noneikonal corrections. The dashed curve was calculated without, the solid line with the noneikonal corrections. They were both calculated with *pp* and *pn* amplitudes of the Gaussian form. The dashed-dotted curve corresponds to the *pp* and *pn* amplitudes taken from phase shift analysis (Ref. 26).

(12) of Ref. 4]. As was pointed out in Ref. 8, the main effect of the noneikonal correction is to change the phases of the successive multiple scattering amplitudes, with the phase factors depending approximately linearly on the momentum transfer squared. Consequently, the noneikonal effects are important in the regions of interference minima in the differential cross section. Their effect on the polarization and spin rotation functions turns out to be much stronger.

The Coulomb interaction can be calculated in a straightforward way in the Glauber model.[3] For an impact parameter $\vec{b}$ it leads us to a phase

$$\chi^C(\vec{b})=\chi_1^C(b)+\vec{\sigma}\cdot\vec{n}_b\chi_2^C(b)\ , \tag{4a}$$

where $\chi_1^C(b)$ and $\chi_2^C(b)$ are central and spin-orbit Coulomb phases, respectively.

Our treatment of Coulomb effects also includes the electromagnetic spin-orbit term as has been recently proposed in Refs. 9 and 10:

$$\chi_1^C(b)=-\frac{1}{v}\int_{-\infty}^{\infty}dz\,V_C(b,z)\ , \tag{4b}$$

$$\chi_2^C(b)=-\xi v\frac{d}{db}\chi_1^C(b)\ , \tag{4c}$$

$$\xi=\frac{1}{2(E+m)}+\frac{\kappa}{2m}\ . \tag{4d}$$

Here $V_C(b,z)$ is the Coulomb potential, v is the relative proton velocity, and $\kappa=1.79$, the anomalous magnetic moment of the proton.

As is well known, the Coulomb field dominates the elastic scattering at small momentum transfers and affects significantly the regions of interference minima in the differential cross section and polarization observables. As for the magnetic moment interaction, it turns out to play a small role everywhere except for the interference region in the po-

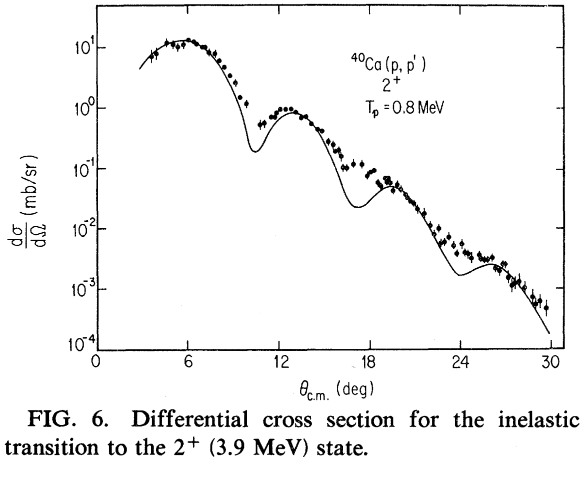

FIG. 6. Differential cross section for the inelastic transition to the 2^+ (3.9 MeV) state.

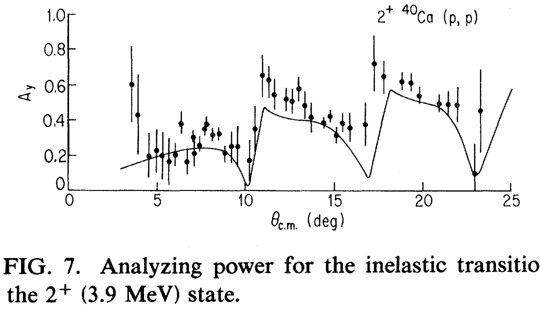

FIG. 7. Analyzing power for the inelastic transition to the 2^+ (3.9 MeV) state.

larization observables at small angles.

The conventional procedure for the treatment of Coulomb effects in the diffraction theory consists of separating out the Coulomb amplitude for scattering from the pointlike charge distribution. Schematically, the profile function

$$\begin{aligned}\Gamma(\vec{b}) &= 1-\exp\{i[\chi^C(\vec{b})+\chi^s(\vec{b})]\}\\ &= \{1-\exp[i\chi^{\mathrm{pt}}(\vec{b})]\}+\exp[i\chi^{\mathrm{pt}}(b)]\\ &\quad\times(1-\exp\{i[\delta\chi^C(\vec{b})+\chi^s(\vec{b})]\})\ ,\end{aligned} \tag{5}$$

where $\delta\chi^C=\chi^C-\chi^{\mathrm{pt}}$, χ^s is the strong interaction phase shift, and χ^{pt} and χ^C are the Coulomb phase shifts for the pointlike and extended charge, respectively. The advantage of this approach is that the first term, the pointlike Coulomb scattering amplitude, can be calculated analytically. However, in the present analysis we are dealing with very large momentum transfers squared, where very strong cancellations between the above two terms occur. Therefore, the latter must be calculated to a very high precision, and this procedure becomes numerically rather awkward. In order to obtain better convergence in the high momentum transfer region, we used the alternative method of Ref. 11 which consists of separating the Coulomb scattering amplitude for the extended charge distribution. In this approach the profile function is written as a sum of two terms:

$$\begin{aligned}\Gamma(b) &= 1-\exp\{i[\chi^C(\vec{b})+\chi^s(\vec{b})]\}\\ &= \{1-\exp[i\chi^C(\vec{b})]\}+\exp[i\chi^C(\vec{b})]\\ &\quad\times\{1-\exp[i\chi^s(\vec{b})]\}\ .\end{aligned} \tag{6}$$

Now the numerical integration of the Fourier transfer [Eq. (1)] of the second term in Eq. (6) is straightforward. The first term, however, owing to the long-range nature of the Coulomb forces, extends outside the nucleus. This difficulty can be removed by extracting explicitly the $1/\Delta^2$ term from the integrand. This method allows one to achieve stability of the numerical results much faster and reduces the computation time considerably.

In order to take into account the c.m. correction, we have used in Eq. (1) the c.m. corrected density defined as:

$$\rho(r_1,\ldots r_A)=\prod_{i=1}^{A}\rho(r_i)\delta(\Sigma r_i)\ ,$$

where $\rho(r_i)$ are the single particle densities. As a result we have obtained (in the zero range force approximation) the c.m. corrected amplitude

$$F^{\mathrm{c.m.}}(\vec{\Delta})=F_1^{\mathrm{c.m.}}(\vec{\Delta})+F_2^{\mathrm{c.m.}}(\vec{\Delta})+\cdots+F_A^{\mathrm{c.m.}}(\vec{\Delta})\ , \tag{7}$$

where $F_1^{\mathrm{c.m.}}$, $F_2^{\mathrm{c.m.}}, \ldots,$ are single, double, etc., scattering amplitudes which are related to the corresponding multiple scattering amplitudes calculated without the c.m. correction in the following way:

$$F_n^{\mathrm{c.m.}}(\vec{\Delta})=\int d^2p\,[\tilde{\rho}(\vec{\mathrm{p}})^{A-n}F_n(\vec{\Delta}+n\vec{\mathrm{p}})\Big/\int d^2p\,[\tilde{\rho}(p)]^A \tag{8}$$

with

$$\tilde{\rho}(p)=\int d^2s\,e^{i\vec{\mathrm{p}}\cdot\vec{\mathrm{s}}}\int dz\,\rho(r)\ .$$

The above formula has been obtained under the assumption that the proton size is much smaller than the target size. The c.m. correction influences separately each particular order of scattering. The total influence of the c.m. correction on the differential cross section we obtained can be, to a good accuracy, approximated by the factor $\exp(0.45\ \Delta^2)$, where Δ^2 is in units of $(\mathrm{GeV}/c)^2$. This result turns out to be in qualitative agreement with the c.m. correlation effect of Refs. 12 and 13.

In order to estimate the corrections due to the short range and Pauli correlations, we have used the standard general expansion of the ground state density in terms of the two-particle, three-particle, etc.,

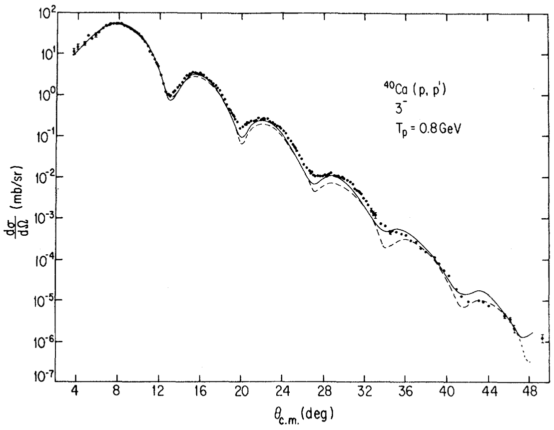

FIG. 8. Differential cross section for the inelastic transition to the 3^- (3.79 MeV) state. The dashed curve was calculated without the spin-orbit term in the N-N amplitude.

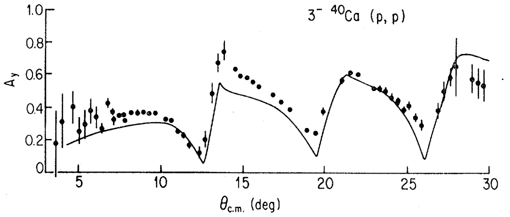

FIG. 9. Analyzing power for the inelastic transition to the 3^- (3.79 MeV) state.

correlations and have neglected terms depending on correlations of order higher than two.[14] In this approximation the density can be written as

$$\rho(\vec{r}_1,\ldots,\vec{r}_A)=\rho(\vec{r}_1)\ldots\rho(\vec{r}_A)+\sum_{\substack{\text{all possible}\\ \text{contractions}}}\Delta[\rho(\vec{r}_1)\ldots\rho(\vec{r}_n)]\ , \qquad (9)$$

where the contraction is defined as:

$$\Delta(\vec{r}_1,\vec{r}_2)=\rho(\vec{r}_1,\vec{r}_2)-\rho(\vec{r}_1)\rho(\vec{r}_2)$$

$$=C(\vec{r}_1,\vec{r}_2)\rho(\vec{r}_1)\rho(\vec{r}_2) \qquad (10)$$

with

$$\rho(\vec{r}_1)=\int d^3r_2\ldots d^3r_A\,\rho(\vec{r}_1,\ldots\vec{r}_A)\ , \qquad (11)$$

and

$$\rho(\vec{r}_1,\vec{r}_2)=\int d^3r_3\ldots d^3r_A\,\rho(\vec{r}_1,\ldots\vec{r}_A)\ .$$

The dimensionless function $C(\vec{r}_1,\vec{r}_2)$ is the two particle correlation function which has the following properties

$$C(\vec{r}_1,\vec{r}_2)\to 0 \text{ for } |\vec{r}_1-\vec{r}_2|\to\infty\ , \qquad (12)$$

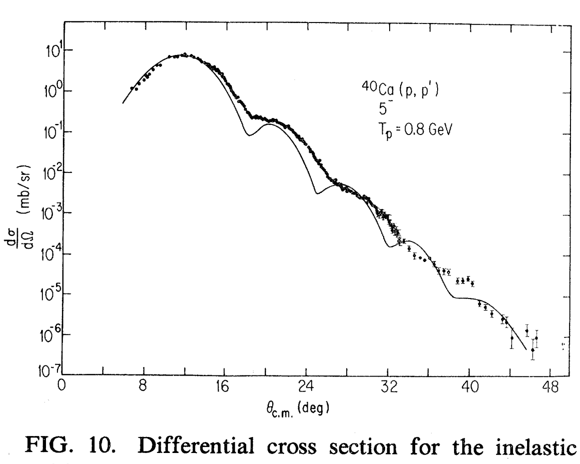

FIG. 10. Differential cross section for the inelastic transition to the 5^- (4.49 MeV) state.

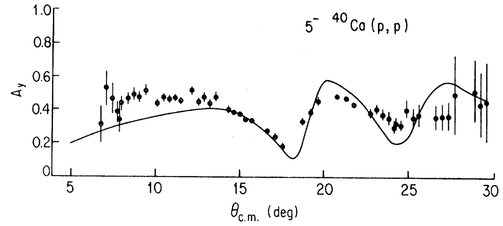

FIG. 11. Analyzing power for the inelastic transition to the 5^- (4.49 MeV) state.

and

$$\int d^3r_1 C(\vec{r}_1,\vec{r}_2)\rho(\vec{r}_1)=0\ .$$

In general, for finite nuclei, the correlation function $C(\vec{r}_1,\vec{r}_2)$ depends not only on the relative distance between the target nucleons but also on their position from the center of the nucleus. One may expect the correlation effects to be weaker near the nucleus surface, where most of the scattering takes place. The exact form of the correlation function

$$C(\vec{r}_1,\vec{r}_2)=C((\vec{r}_1+\vec{r}_2)/2),((\vec{r}_1-\vec{r}_2)/2)$$

is known only for some special cases, e.g., for the noninteracting Fermi gas model.

In this paper, following Ref. 15, we have expressed the correlation effect in terms of the effective correlation length ξ_c smeared out with the spatial distribution of the projectile-nucleon interaction:

$$\xi_c=\frac{1}{4\pi a}\int d^2s\int dz\,C(s,z)\exp[-s^2/4a]\ . \qquad (13)$$

[Note that ξ_c reduces to the correlation length[14]

$$l_c=\int d^3s\int dz\,C(s,z)\ , \qquad (14)$$

where $l_c \gg a$.]

We assumed that the correlation function depends only on the relative distance between the two nucleons. In doing so we hope not to oversimplify the problem. The existing calculations of correlation effects within the framework of the Glauber model[16] seem to be insensitive to the particular form of the correlation function and depend mainly on l_c.

Various authors give different estimates for l_c, varying from -0.3 fm (Ref. 17) to -0.85 fm.[16] Note that they are all negative, which, as can be seen from the definition of l_c [see Eq. (14)], indicates a repulsive force at small distances.

2. *Proton and neutron density distribution and proton-nucleon amplitudes used in the analysis*

For our calculation, the proton point density distribution $\rho_p(r)$ was obtained from an analysis of electron scattering on ^{40}Ca.[18] Following Ref. 18 we adopted the following form of $\rho_p(r)$:

$$\rho_p(r)=\rho_0\left\{\frac{1+(w_p/R_p{}^2)r^2}{1+\exp[(r-R_p)/a_p]}+a_0\frac{\sin q_0 r}{q_0 r}\exp[-p_0{}^2(r^2/4)]\right\}. \qquad (15a)$$

The parameters of $\rho_p(r)$ are listed in Table I.

We used a three parameter Fermi distribution

$$\rho_n(r)=\rho_0[1+(w_n/R_n{}^2)r^2]/\{1+\exp[(r-R_n)/a_n]\} \qquad (15b)$$

to describe the neutron density. The parameters were varied to obtain the best fit to the $p+{}^{40}$Ca data.

As for the nucleon-nucleon input to our calculation, we have taken into account only two components of the N-N amplitude, using the following standard parametrization

$$f_{NN}(q)=f_{NN}^c(q)+\vec{\sigma}\cdot(\vec{q}\times\hat{k})f_{NN}^s(q)\,, \qquad (16)$$

i.e., we keep only terms which do not cause spin flip transitions of the target nucleons. The other terms are strongly suppressed in the case of proton scattering from reasonably heavy nuclei of spin zero. In Eq. (16), $f_{NN}^c(q)$ and $f_{NN}^s(q)$ are the central and spin orbit N-N amplitudes, $\vec{\sigma}$ stands for the projectile spin $\frac{1}{2}$ operator. We parametrized $f_{NN}^c(q)$ and $f_{NN}^s(q)$ in terms of Gaussians in one set of calculations, whereas in a second set of calculations we used more realistic amplitudes obtained from phase shift analyses. These will be discussed below.

The central and spin-orbit parts of the *pp* and *pn* amplitudes, in our first set of calculations, were parametrized as

$$f_{pp(pn)}^c=\frac{k\sigma_{pp(pn)}}{4\pi}(i+\alpha_{pp(pn)})\times\exp\left[-\frac{\beta_{pp(pn)}}{2}q^2\right], \qquad (17a)$$

$$f_{pp(pn)}^s=\frac{k\lambda_{pp(pn)}}{4\pi}(i+\alpha_{pp(pn)}^s)\times\exp\left[-\frac{\beta_{pp(pn)}^s}{2}q^2\right]. \qquad (17b)$$

We assumed that the spin-dependent amplitudes for *p*-*p* and *p*-*n* are equal. Table II lists the parameters used in Eqs. (17a) and (17b). The parameters for the spin independent part were derived from the compilation of Bystricky *et al.*[19] and are in reasonable agreement with those used by Blanpied *et al.*[20] The parameters of the spin dependent part (also listed in Table II) were adjusted to obtain a best fit to the p-^{40}Ca analyzing power data (see Fig. 5).

TABLE I. Proton density parameters used in the calculation [Eq. (15a)].

$a_p=0.59$ fm $\qquad a_0=0.081$
$R_p=3.77$ fm $\qquad p_0=0.43$ fm^{-1}
$w=-0.161$ $\qquad q_0=3.14$ fm^{-1}
$\langle r_p{}^2\rangle^{1/2}=3.482$ fm

TABLE II. Parameters of the *NN* amplitudes [Eq. (17)].

$\sigma_{pp}=4.73$ fm^2 $\qquad \sigma_{pn}=3.80$ fm^2
$\alpha_{pp}=0.056$ $\qquad \alpha_{pn}=0.20$
$\beta_{pp}=(0.18-i0.05)$ fm^2 $\qquad \beta_{pn}=(0.24-i0.05)$ fm^2
$\lambda_{pp}=\lambda_{pn}=0.81$ fm^3
$\alpha_{pp}^s=\alpha_{pn}^s=-1.0$
$\beta_{pp}^s=\beta_{pn}^s=0.6$ fm^2

3. *Discussion of the effects of noneikonal corrections, spin-orbit effects, and correlations on the elastic scattering*

In this section we discuss the sensitivity of the elastic scattering calculations to noneikonal corrections, the spin-orbit part of the *NN* amplitude, and the nucleon-nucleon correlations within the context of the diffraction multiple scattering theory.

Noneikonal correction and the spin-orbit effects reduce the amplitude of oscillation without changing the phase of the oscillation in the differential cross section and polarization, whereas correlations cause a q dependent change in phase. The first

TABLE III. Parameters of the extracted neutron density [Eq. (15b)].

$a_{nn}=0.51$ fm $\qquad R_n=3.45$ fm $\qquad w_n=0.108$
$\langle r_n{}^2\rangle^{1/2}=3.34$ fm

mentioned effects increase the spin independent and spin orbit projectile-nucleus amplitudes (double spin flip terms were neglected because, as it was shown in Ref. 9, their role is negligible).

The important feature, displayed in Figs. 12 and 13, is that noneikonal effects, spin effects, and correlations play a minor role for $\theta_{\mathrm{c.m.}} \leq 20°$. Thus the data from 2–20° are most unambiguously related to the neutron mass distribution and the difference in rms radii of the proton and neutron point mass distributions, $\langle r_p{}^2\rangle^{1/2} - \langle r_n{}^2\rangle^{1/2}$. The data at angles of $20° \leq \theta_{\mathrm{c.m.}} < 42°$ are useful for investigating the size of the correlation range parameters ξ_c, since having fixed parameters of the proton and neutron point mass distributions an effective ξ_c can be determined by adjustment of the phase to match the experimental data. The amplitude of the large angle data, i.e., the height of the maximum and depth of the minimum, is sensitive to spin-orbit effects and to the noneikonal corrections. Figures 4 and 5 (solid line) show that a very satisfactory fit to the data is obtained. The parameters describing the Fermi shape of the point neutron mass distribution are listed in Table III. They yield a rms radius $\langle r_n{}^2\rangle^{1/2}$ of 3.34±0.05 fm. The value of $\langle r_p{}^2\rangle^{1/2}$ from Ref. 18 is 3.482±0.025 fm and $\langle r_p{}^2\rangle^{1/2} - \langle r_n{}^2\rangle^{1/2} = 0.142 \pm 0.075$. The proton radius excess for ^{40}Ca can be ascribed to the Coulomb repulsive forces pushing the protons away from each other.

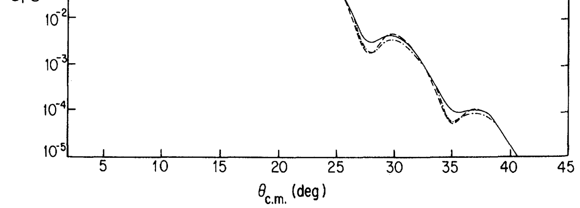

FIG. 12. Effect of the noneikonal corrections and spin effects for the p-^{40}Ca elastic differential cross section. The dashed line was obtained without the noneikonal corrections. The dotted line was calculated without the spin orbit term in the N-N amplitude.

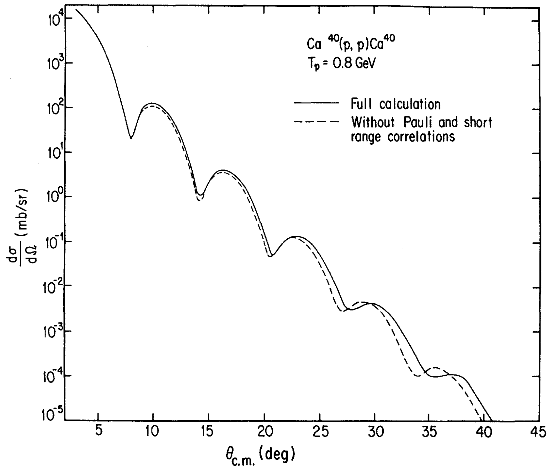

FIG. 13. Effect of correlations on the p-^{40}Ca elastic differential cross section. Solid and dashed curves are calculated with $\xi_c = -0.5$ fm and $\xi_c = 0$, respectively.

Within the error corridor our results are in agreement with the previous Glauber theory analysis[21] carried out in the smaller ($\theta_{\mathrm{c.m.}} \leq 16°$) momentum transfer region. The results of the numerous Hartree-Fock calculations are slightly but consistently lower. The density dependent Hartree-Fock theory[22] gives 0.04, the Hartree-Fock calculation using Skyrme's II interaction[23] yields 0.05, and the density matrix expansion[24] provides 0.05 for the difference between the proton and neutron radii. The existing Kerman, McManus, and Thaler (KMT) analyses carried out in the smaller (up to $\theta_{\mathrm{c.m.}} = 24°$) momentum transfer region yield $\langle r_p{}^2\rangle^{1/2} - \langle r_n{}^2\rangle^{1/2} = 0.15$ and 0.17 fm (calculation of the 800 MeV p-^{40}Ca scattering[2] with NN amplitudes of the Gaussian type and taken from the phase shift analysis, respectively) and $\langle r_p{}^2\rangle^{1/2} - \langle r_n{}^2\rangle^{1/2} = 0.04$ (calculation of the 1 GeV p-^{40}Ca scattering[25] with N-N amplitudes of the Gaussian form). Our evaluation of the noneikonal correction and a realistic estimate of the spin-orbit effects reproduce quite well the observed attenuation in amplitude seen in both the cross section and analyzing power data at large angles. A value of −0.5 fm for the correlation range parameter ξ_c produces the observed change in phase at large angles. This value is well within the bounds indicated by earlier Glauber theory analyses, −0.3 fm (Ref. 17) to −0.85 fm.[16]

The dashed-dotted curves in Figs. 4 and 5 correspond to the differential cross section and polarization observables calculated with the N-N amplitudes available from phase shift analyses.[26] The most striking feature is that the polarization observable does not display now as strong a structure as it does when calculated with the Gaussian amplitudes. It can be attributed to the fact that the slopes of the central and spin-orbit parts of the *N*-*N* amplitudes obtained by phase shift analyses do not differ much at small momentum transfers. The leading contribution to the oscillating structure of the polarization is due, as discussed in Ref. 27, to the slope difference between the central and spin-orbit parts of the *N*-*N* amplitude, and for heavier nuclei, to Coulomb effects. When the Coulomb interaction is neglected, and $\beta^s-\beta=0$, there are no oscillations in proton-nucleus polarization, and its shape becomes the same as in proton-nucleon scattering. A similar tendency has been found when the *N*-*N* amplitudes from phase shift analyses were used in analyzing the analyzing power and spin rotation observables at 500 MeV for p-^{40}Ca scattering.[28]

Referring back to Fig. 5 we see that the theoretical prediction for the analyzing power using *N*-*N* amplitudes obtained from phase shift analysis displays quantitatively some lack of agreement with the experimental data. This discrepancy may still be attributable to the fact that most of the *N*-*N* input data used in the phase shift analysis comes from the region of $-t \geq 0.1$ (GeV/c)^2 (i.e., 15° in the laboratory system). However, because of the rapid falloff of the nuclear form factor, the amplitude for elastic scattering from a large nucleus is sensitive mostly to the *N*-*N* amplitudes at very small momentum transfers. We believe that there is still enough ambiguity in the *N*-*N* amplitudes to improve the agreement of the theory with the data.

B. Inelastic scattering

We have carried out the theoretical analysis of the data for the inelastic scattering in the framework of the Glauber diffraction theory.[3] In this approach the amplitude for the proton induced inelastic transition to a level of excitation energy much smaller than the projectile energy can be calculated using as input the free nucleon-nucleon amplitude and the corresponding inelastic transition density. Following Refs. 29 and 30 we have treated the excited levels of ^{40}Ca as collective excitations of the adiabatic type,[31] taking into account only terms linear in the deformation parameter. This assumption corresponds to the one phonon excitation mechanism. The corresponding transition density is then simply[32]

$$\rho_{\rm tr}(R)=\beta_L R\frac{d}{dr}\rho(r)Y_{LM}(\hat{r})\ , \tag{18}$$

where β_L is the transition strength. The equal density surfaces were assumed to be the same for all nucleons and parametrized as two-parameter Fermi distributions,

$$\rho(r)=\rho_0/\{1+\exp[(r-R)/a]\}\ , \tag{19}$$

with $R=3.51$ fm and $a=0.56$ fm. These parameters give an rms value of 3.52 fm, which is approximately equal to the average of the rms values of the ground state proton and neutron densities used in our calculation of the elastic scattering.

As in the case of elastic scattering, we used the spin dependent nucleon-nucleon amplitude of Eq. (1). In contrast with previous Glauber model analyses of inelastic transitions for heavier nuclei where the spin effects were either not treated or calculated in the zero-force range approximation [$\beta=\beta^s=0$ in Eq. (17)],[29,30] we took into account the momentum dependence of the spin orbit amplitude. (Coulomb and center-of-mass effects were treated analogously as in the elastic scattering.)

In Figs. 6 — 11 we display our results for differential cross sections and analyzing powers. In these calculations, we used an isospin-averaged *N*-*N* amplitude with the following parametrization of its central and spin orbit parts[16]:

$$\begin{aligned} f^c(q)&=\frac{k\sigma}{4\pi}(i+\alpha)\exp[-(\beta/2)q^2]\ ,\\ f^s(q)&=\frac{k\lambda}{4\pi}(i+\alpha^s)\exp[-(\beta^s/2)q^2]\ . \end{aligned} \tag{20}$$

For the forward amplitude $f^c(0)$ and the corresponding slope, we took parameters as determined from Ref. 33. They are listed in Table IV, column 1. The parameters describing the spin orbit part of the isospin averaged Gaussian amplitude were adjusted to obtain the best fit to the inelastic data. The values obtained are listed in Table IV, column 2.

The corresponding transition strengths β_L are listed in Table V. The transition strengths β_2, β_3, β_5 agree with those obtained from low energy electron scattering experiments.[34,35] They also agree with results obtained from the analysis of Starodubsky[29] of the data obtained by Alkhazov *et al.*[36] for

TABLE IV. Isospin averaged *N*-*N* amplitudes used in the analysis of the inelastic scattering [Eq. (20)].

$\sigma=4.4$ fm^2	$\lambda=0.89$ fm^3
$\alpha=0.28$	$\alpha^s=-1.0$
$\beta=0.21$ fm^{-2}	$\beta^s=0.45$ fm^2

TABLE V. Comparison of the transition strengths β_L used in the present paper with those used in Ref. 29.

	Ref. 29	This work
β_2	0.132	0.133
β_3	0.38	0.340
β_5	0.22	0.215

the smaller momentum range (see Table V for comparison).

We have found that the contribution of the spin orbit part of the *N-N* amplitude is more important for the inelastic differential cross sections than for the elastic cross section. The effect is to enhance the subsidiary diffractive maxima in the differential cross section by 60% starting from about 30° in the c.m.f. In Fig. 8 we illustrate this effect for the case of the excitation of the 3^- state. The dashed line has been obtained by putting $f^s(q)$ [see Eq. (3)] equal to zero, whereas the solid line corresponds to the full calculation with $f^s(q)\neq 0$. The overall agreement between theory and data is remarkably good given the simplicity of our assumptions about the transition densities. We might expect further improvements if we were to add the higher order terms of the transition density expansions, i.e., terms describing the two-phonon excitations. Such contributions are probably of more importance for the 5^- transition.

Noneikonal effects (which have not been included in the inelastic case) may be much stronger for the inelastic transitions, in particular, in the regions of diffractive minima, which would become less sharp if this correction were taken into account.

We conclude that the large angle inelastic data can be qualitatively reproduced by our simple calculation. The 5^- transition is least well described, and we attribute this to the importance of two-phonon transitions which are not included in this analysis.

IV. CONCLUSION AND SUMMARY

We have presented here new, large momentum transfer data for elastic and inelastic scattering of 800 MeV protons from ^{40}Ca. The present experiment covers a considerably larger angular range than the previous measurements which extended only out to 24° in the c.m.f.[1,2] The elastic scattering observables, differential cross section, and analyzing power, were analyzed using the noneikonal extension[4] of the Glauber diffraction theory.

A comment is in order here regarding the applicability of the Glauber theory, which is essentially a high energy, small scattering angle approximation. In the multiple scattering picture the amplitude for *p*-nucleus scattering is given as a sum of various multiple scattering terms. The importance of the higher order multiple scattering terms increases with the growing momentum transfer because of the strong exponential dependence of the nuclear form factor on the momentum transfer squared. One can easily show that the most probable contribution for the *n*th order multiple scattering term comes from the situation in which the overall momentum transfer is equally shared between the momentum transfers acquired by the projectile on the target nucleons. Hence the scattering process which proceeds as a series of small angle scatterings on individual nucleons can be suitably described by the diffraction theory. The noneikonal effects which take into account the deviations from the straight-line propagation picture produce further improvement of the model at intermediate energies.

One of the additional advantages of the Glauber theory is that the effects of center-of-mass, short range, and Pauli correlations can be calculated microscopically without using the exponentiation procedure (optical limit) which is mathematically dangerous in the region of large momentum transfers where the corrections become sizable. The proton density distribution used as input in our calculations reproduces the ^{40}Ca elastic form factor measured in the e-^{40}Ca experiment.[18]

From our analysis of the proton scattering data for $\theta_{\mathrm{c.m.}} < 20°$ it follows that the best agreement between experiment and theory can be obtained with the neutron density rms radius smaller than the proton distribution by about 0.15 fm. Larger angle data (out to $\theta_{\mathrm{c.m.}} = 42°$) indicate the effective correlation range parameter to be as $\xi_c = -0.5$ fm.

The inelastic transitions were treated in our calculations as collective excitations of the adiabatic type. The low-lying 2^+ and 3^- inelastic transitions are well described macroscopically by the transition strength parameters β_L and a one-phonon excitation mechanism. The differential cross section for the lowest lying 5^- excitation is not described as well. We point out that two-phonon excitation (not included in the calculations reported here) should be included.

The momentum dependence of the spin-orbit part of the nucleon-nucleon amplitude plays an important role in the inelastic scattering observables. Earlier Glauber theory analyses have not included the spin-orbit term or have used a zero range spin-orbit amplitude.[29,30] Starting from 30° c.m. the spin effects enhance the subsidiary maxima in the inelastic distribution by about 60%. The slope difference between the central and spin-orbit part of the N-N amplitude very strongly influences (sharpens) the shape of the analyzing power.

This work was supported in part by the U. S. Department of Energy, Washington, D.C., and by the Robert A. Welch Foundation.

---

[*] Now at Los Alamos National Laboratory, Los Alamos, New Mexico 87545.

[†] Now at Bates Laboratory, Massachusetts Institute of Technology, Cambridge, Massachusetts 02139.

[‡] Now at Schweizerisches Institut für Nuklearforschung, 5234 Villigen, Switzerland.

[1] G. Igo *et al.*, Phys. Lett. 81B, 159 (1979).

[2] L. Ray *et al.*, Phys. Rev. C 23, 828 (1981).

[3] R. Glauber, in *Lectures in Theoretical Physics,* edited by W. E. Britten *et al.* (Interscience, New York, 1959), Vol. 1, p. 315.

[4] M. Bleszynski and P. Osland, Phys. Lett. 84B, 157 (1979).

[5] G. W. Hoffmann *et al.*, Phys. Rev. C 21, 1488 (1980).

[6] G. W. Hoffmann *et al.*, Phys. Rev. C (in press).

[7] G. Adams *et al.*, Phys. Rev. C 21, 2485 (1980).

[8] M. Bleszynski and T. Jaroszewicz, Phys. Lett. 56B, 427 (1975).

[9] P. Osland and R. Glauber, Nucl. Phys. A326, 255 (1979).

[10] G. Fäldt and G. Ingemarsson, The Gustaf Werner Institute Report GWI-PH 5/81.

[11] G. Fäldt and I. Hulthage, Nucl. Phys. A302, 433 (1978).

[12] D. Harrington and K. Varma, Nucl. Phys. A306, 477 (1978).

[13] J. P. Auger and R. Lombard, J. Phys. G 4, L261 (1978).

[14] S. Foldy and J. D. Walecka, Ann. Phys. (N.Y.) 54, 447 (1969).

[15] E. Bleszynski, M. Bleszynski, and W. Czyz, Acta Phys. Pol. B8, 393 (1977).

[16] E. J. Moniz and G. D. Nixon, Ann. Phys. (N.Y.) 67, 58 (1971).

[17] D. R. Yennie, in *Hadronic Interactions of Electrons and Photons,* edited by J. Cummings and H. Osborn (Academic, New York, 1971), p. 321.

[18] B. B. P. Sinha *et al.*, Phys. Rev. C 7, 1930 (1973).

[19] J. Bystricky *et al.*, Centre d'Etudes Nucléaires de Saclay, Report No. CEA-N1547CE, 1972.

[20] G. S. Blanpied *et al.*, Phys. Rev. Lett. 39, 1447 (1977).

[21] G. K. Varma and L. Zamick, Phys. Rev. C 16, 308 (1977).

[22] J. W. Negele, Phys. Rev. C 1, 1260 (1970).

[23] D. Vautherin and D. Brink, Phys. Rev. C 5, 626 (1972).

[24] J. W. Negele and D. Vautherin, Phys. Rev. C 5, 1472 (1972).

[25] A. Chaumeaux, V. Layly, and R. Schaeffer, Phys. Lett. 75B, 33 (1977); Ann. Phys. (N.Y.) 116, 247 (1978).

[26] D. Arndt, private communication.

[27] G. Fäldt and A. Ingemarsson, The Gustaf Werner Institute Report GWI-PH 2/81.

[28] A. Rahbar *et al.*, Phys. Rev. Lett. 47, 1811 (1981).

[29] V. E. Starodubsky, Nucl. Phys. A219, 525 (1974); Leningrad Nuclear Institute Report No. 443, 1978.

[30] G. Fäldt and P. Osland, Nucl. Phys. A305, 509 (1978).

[31] A. Bohr and B. R. Mottelson, *Nuclear Structure* (Benjamin, Reading, Mass., 1975), Vol. 2, p. 654.

[32] L. J. Tassie, Aust. J. Phys. 9, 407 (1956); G. E. Satchler, Phys. Rep. 14C, 99 (1979).

[33] D. V. Bugg *et al.*, Phys. Rev. 146, 980 (1966).

[34] R. A. Eisenstein *et al.*, Phys. Rev. 188, 1915 (1969).

[35] K. Itoh *et al.*, Phys. Rev. C 2, 2181 (1970); R. E. Frosch *et al.*, Phys. Rev. 179, 1380 (1968).

[36] G. D. Alkhazov *et al.*, Nucl. Phys. A247, 443 (1976).

[37] See AIP document No. PRVCA-25-2563-19 for 19 pages of numerical data for 0.8 GeV scattering of protons from ^{40}Ca. Order by PAPS number and journal reference from American Institute of Physics, Physics Auxiliary Publication Service, 335 East 45th Street, New York, NY 10017. The prices are $1.50 for microfiche or $5 for photocopies. Airmail additional. Make checks payable to the American Institute of Physics.